Long-Wavelength $In_{0.53}Ga_{0.47}As$–$In_{0.52}Al_{0.48}As$ Large-Area Avalanche Photodiodes and Arrays

X. G. Zheng, J. S. Hsu, J. B. Hurst, X. Li, S. Wang, X. Sun, Archie L. Holmes, Jr., *Member, IEEE*, Joe C. Campbell, *Fellow, IEEE*, Andrew S. Huntington, and Larry A. Coldren, *Fellow, IEEE*

***Abstract*—Large-area (500-μm diameter) mesa-structure $In_{0.53}Ga_{0.47}As$–$In_{0.52}Al_{0.48}As$ avalanche photodiodes (APDs) are reported. The dark current density was $\sim 2.5\times10^{-2}$ nA/μm^2 at 90% of breakdown; low surface leakage current density ($\sim$4.2 pA/μm) was achieved with wet chemical etching and SiO_2 passivation. An 18 $\times$ 18 APD array with uniform distributions of breakdown voltage, dark current, and multiplication gain has also been demonstrated. The APDs in the array achieved 3-dB bandwidth of $\sim$8 GHz at low gain and a gain-bandwidth product of $\sim$120 GHz.**

***Index Terms*—Avalanche multiplication, avalanche photodiodes, excess noise factor, impact ionization, ionization coefficient, photodetectors, photodiode.**

I. Introduction

THE $In_{0.53}Ga_{0.47}As$–$In_{0.52}Al_{0.48}As$ avalanche photodiodes (APDs) have been widely studied for wide-band optical communication applications. Much of the research on these APDs has focused on achieving higher gain-bandwidth products to accommodate the ever-increasing bit rates of fiber-optic systems. For this application, small device size is preferred in order to reduce the RC time constant. On the other hand, emerging optical measurement systems that operate in the eye-safety wavelength range ($\sim$ 1.5 μm) require long-wavelength, high-sensitivity photodiodes with large detection area. For many applications of this type an APD is preferable to a p-i-n photodiode since the internal gain of the APD affords higher sensitivity. Good material uniformity is required by three-dimensional infrared imaging systems, which utilize APD arrays that operate in the short-wavelength infrared (SWIR) range (0.8 μm $\leq \lambda \leq$ 2.2 μm) and have gigahertz bandwidths [1]. Both applications present stringent challenges to the quality and uniformity of the epitaxial layers from which the APDs are fabricated. In addition, passivation of the InP-based material is critical. If large defect densities are created during material growth (MBE or MOCVD), the bulk leakage current will be high, severe microplasma-induced speed degradation will result [2], and the device reliability for large-area APDs and arrays will suffer [3]. From a processing point of view, the quality of device passivation is critical if low dark currents are to be achieved [4]. Previously, a 100-μm-diameter InAlGaAs-InAlAs super-lattice APD integrated with a 200-μm diameter microlens has been reported for eye-safe optical measurements [5]. In this paper, we report $In_{0.53}Ga_{0.47}As$–$In_{0.52}Al_{0.48}As$ long-wavelength APDs with mesa diameter up to 500 μm. The multiplied dark current density was $\sim$ 2.5 $\times$ 10^{-2} nA/μm^2 at 90% of breakdown. An 18 $\times$ 18 APD array has also been demonstrated with the same InP-based material. This APD array exhibited uniform distributions of breakdown voltage, dark current, and multiplication gain. The APDs in the array demonstrated bandwidth of $\sim$8 GHz at low gains and a gain-bandwidth product of $\sim$120 GHz.

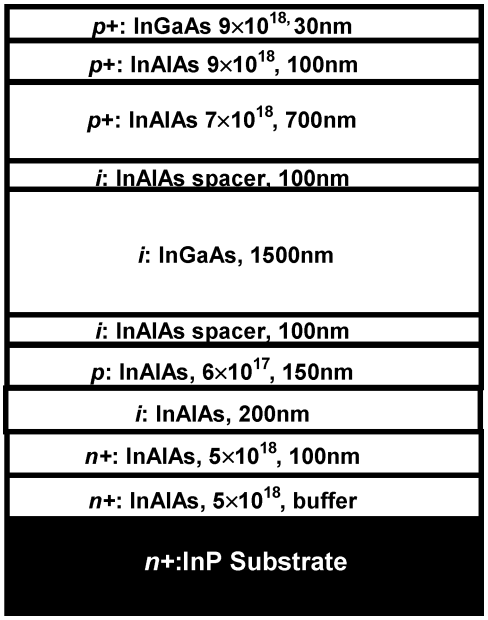

Fig. 1. Device structure for large-area APDs and arrays.

II. Experiment

The separate absorption, charge, and multiplication (SACM) structure that was utilized for the large-area APDs and APD arrays is shown in Fig. 1. This type of device structure typically exhibits low dark current, low multiplication noise, and broad bandwidth if the electric field profile in the entire depleted region is adequately optimized [6]–[10]. A previous report on an $In_{0.53}Ga_{0.47}As$–$In_{0.52}Al_{0.48}As$ 12 $\times$ 12 APD array has demonstrated that long-wavelength APD arrays are achievable based

Manuscript received December 2, 2003; revised April 20, 2004. This work was supported by the Defense Advanced Research Projects Agency through the Heterogeneous Optoelectronics Technology Center and the 3-D Imaging Program.

X. G. Zheng, J. S. Hsu, J. B. Hurst, X. Li, S. Wang, X. Sun, A. L. Holmes, Jr., and J. C. Campbell are with the Department of Electrical and Computer Engineering, Microelectronics Research Center, University of Texas, Austin, TX 78712 USA (email: jcc@mail.utexas.edu).

A. S. Huntington and L. A. Coldren are with the Materials Department, Optoelectronics Technology Center, University of California, Santa Barbara, CA 93106 USA.

Digital Object Identifier 10.1109/JQE.2004.831637

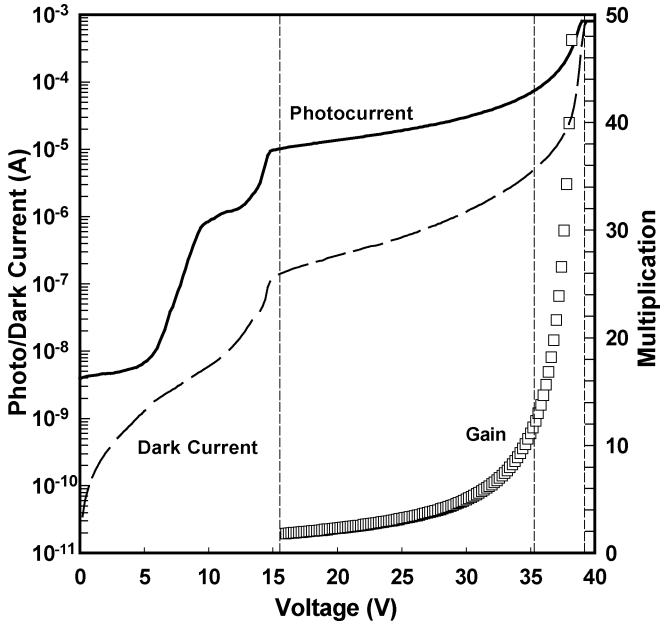

Fig. 2. I–V curves for a 500-μm-mesa-diameter APD.

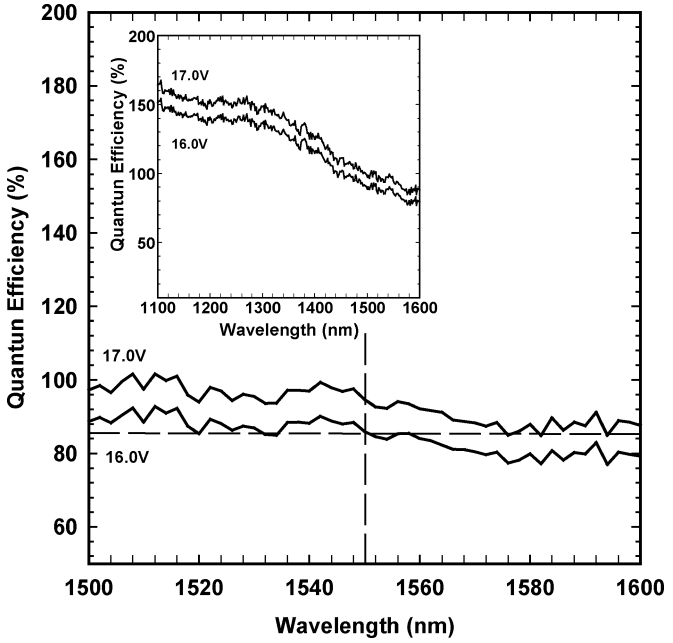

Fig. 3. External quantum efficiency versus wavelength at bias levels of 16.0 and 17.0 V.

on state-of-the-art MBE epitaxial technology, but the speed performance of the 12 × 12 APD array was not satisfactory due to carrier multiplication in the $In_{0.53}Ga_{0.47}As$ absorber [11]. This can be alleviated, to a great extent, by reducing the electric field in the $In_{0.53}Ga_{0.47}As$ absorber. This will also provide the added benefit of reducing the generation-recombination component of the dark current in the absorber, which is the dominant dark current mechanism. In this paper, the charge layer doping has been adjusted to reduce the field in the absorption layer to $<$150 kV/cm. The improved APD wafer structure, as shown in Fig. 1, was grown by molecular beam epitaxy on n-type InP substrates. Detailed material growth conditions and device processing procedures can be found in the previous paper [11].

III. Results and Discussion

A. Large-Area InGaAs–InAlAs APDs

The typical photoresponse and dark current curves of a 500-μm-diameter APD are shown in Fig. 2. The punch-through voltage was ∼15.0 V and the breakdown voltage was ∼39.2 V. The photocurrent was not flat above the punch-through voltage, an indication that gain has been achieved prior to punch-through [2]. In order to estimate the gain, the external quantum efficiency was measured [11] at different biases above punch-through. Fig. 3 shows the quantum efficiency versus wavelength at bias voltages of V = 16.0 and 17.0 V. For bias voltage of 16.0 V, the APD is clearly beyond punch-through and the external quantum efficiency was ∼85% at the wavelength of 1.55 μm, which is much higher than that of previous APD array devices [11], where the unity-gain external quantum efficiency was ∼45% at 1.55 μm. The only difference between these device structures was the charge layer doping level; the large-area APD device has ∼1.85 times higher Be doping concentration in the charge layer. This APD array result can be utilized as a reliable reference for unity-gain quantum efficiency since the APD array device in [11] exhibited very flat photoresponse after punch-through and no obvious gain-enhanced quantum efficiency was observed. Based on this reference the gain at bias voltage of 16.0 V can be estimated as $\geq$1.8. The assertion of gain at punch-through can be also corroborated by an estimate of the electric field intensity. At a reverse bias of 16.0 V, the electric field in the $In_{0.52}Al_{0.48}As$ multiplication region is ∼580 kV/cm, assuming a 200-nm $In_{0.52}Al_{0.48}As$ undoped multiplication region and a 150-nm p-type (6×10^{17} cm^{-3}) $In_{0.52}Al_{0.48}As$ charge region. This value of electric field is consistent with measurements on $In_{0.52}Al_{0.48}As$ homojunction APDs [12], from which it was found that the electric field in a 200-nm-thick multiplication region at gain of 1.8 was ∼560 kV/cm.

The gain of the APD versus voltage was determined using the expression

$$M^* = \frac{I_p - I_d}{I_{pu} - I_{du}}, \quad M = M_0 \cdot M^* \tag{1}$$

where M_0 is the gain factor determined from the quantum efficiency measurement ($M_0 = 1.8$), I_p and I_d are the photocurrent and dark current for bias values above the reference voltage (16 V in this case), I_{pu} and I_{du} are the primary photocurrent and dark current at the reference voltage, M^* is the gain from the I–V measurement, and M is the estimated gain of the APD. The gain curve of a 500-μm-diameter APD is plotted in Fig. 2. APDs having a wide range of mesa diameter (from 20 to 500 μm) exhibited gain values above 40.

The dark current versus voltage curves for APDs with mesa diameters in the range from 20 to 500 μm are shown in Fig. 4. The dark current of the 30-μm-diameter APD was ∼26.7 nA at bias voltage of 35.2 V (90% of the breakdown where gain $>$10). This compares favorably with SiN_x-passivated APDs: 0.7 μA/30 μm by Kagawa *et al.* [13], 0.41 μA/30 μm by Kim *et al.* [3], 0.4 μA/80 μm by Makita *et al.* [14], and the polyimide-passivated APDs (67 nA/30 μm) and the

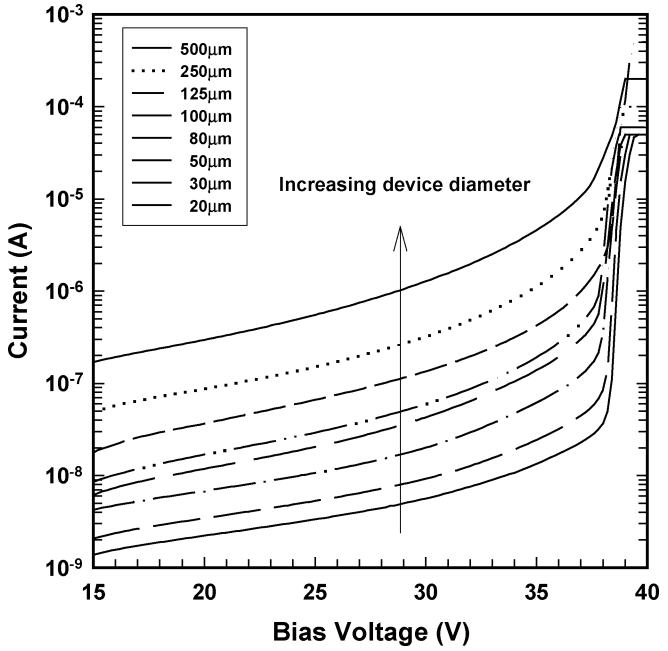

Fig. 4. Dark current versus voltage for APDs with mesa diameters in the range 20–500 μm.

BCB-passivated APDs (38 nA/30 μm) reported by Kim *et al.* [3].

The APD dark current consists of the bulk leakage current, which is proportional to the mesa area, and the sidewall leakage current, which is only proportional to the mesa perimeter. The total dark current can be expressed as

$$I_{\text{total}} = J_{\text{sidewall}} \cdot \pi \cdot d + \frac{J_{\text{bulk}} \cdot \pi \cdot d^2}{4} \tag{2}$$

where J_{sidewall} is the sidewall leakage current density (A/m) and J_{bulk} is the bulk leakage current density (Am^2). The measured dark currents at bias voltage of $\sim$35.2 V (90% of breakdown) are plotted in Fig. 5(a) versus mesa diameter. The solid line is a quadratic fit, which shows that the bulk component of the dark current is dominant. From the fit, the surface dark current density, J_{sidewall}, was 0.19 nA/μm and the bulk dark current density was 0.023 nA/μm^2. The total dark current can also be expressed in terms of the multiplied dark current and unmultiplied dark current using the relation

$$I_{\text{total}} = I_{\text{unmultiplied}} + I_{\text{multiplied}} \cdot M. \tag{3}$$

In Fig. 5(b), (3) was fitted to the dark current of a 100-μm -diameter APD. The unmultiplied dark current (density) was $\sim$1.32 nA (4.2 pA/μm) and the multiplied dark current was $\sim$1.54 nA. The dependence of dark current on gain remains linear to gain values >50. The low value of the unmultiplied dark current (density) is an indication of good material quality and surface passivation; it can be neglected for APDs biased at high gains.

The spatial photoresponse profile of the large-mesa-area APD was measured by the raster-scanning technique. A 1.5-μm-wavelength He–Ne laser beam with a beam-waist <5-μm was scanned across a 500-μm-diameter APD at bias voltage of 36.8 V ($M \sim 20$). A flat, uniform photoresponse profile was obtained across the whole mesa area, as shown in Fig. 6. No spikes in the interior or edge peaks were observed.

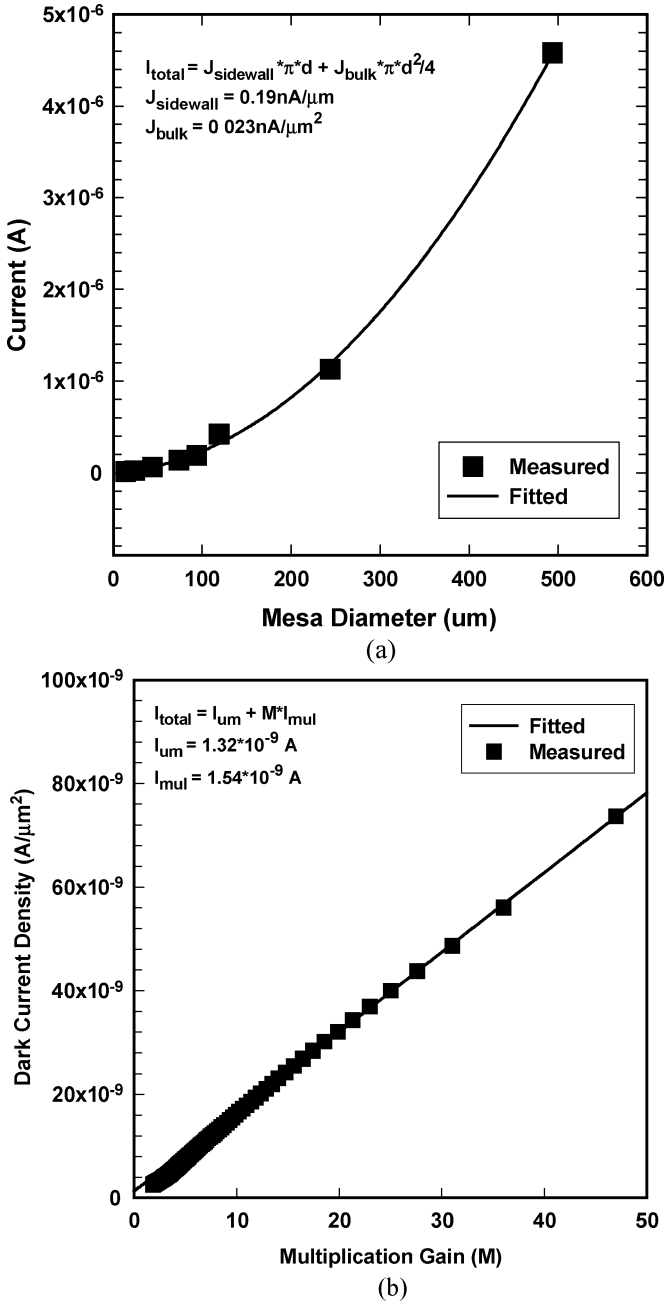

Fig. 5. (a) Dark current and quadratic fit as a function of mesa diameter. (b) Dark current and quadratic fit as a function of gain for a 100-μm device.

B. InGaAs–InAlAs APD Arrays

The photocurrent, dark current, and gain of each device in an 18 × 18 array of 50-μm-diameter APDs were measured. Three devices on the array failed due to improper probing. Statistical analysis of the dark current for the other 321 devices exhibited a mean value of $\sim$4.4 nA and a standard deviation of 1.5 nA at a bias voltage of 16.0 V (gain $\sim$1.8). The dark current distribution at 90% of the breakdown exhibited a mean value of $\sim$71 nA and a standard deviation of 13 nA. The higher fractional spread at higher bias was due to poor sidewall passivation on several devices. Uniform photocurrent was consistently observed across

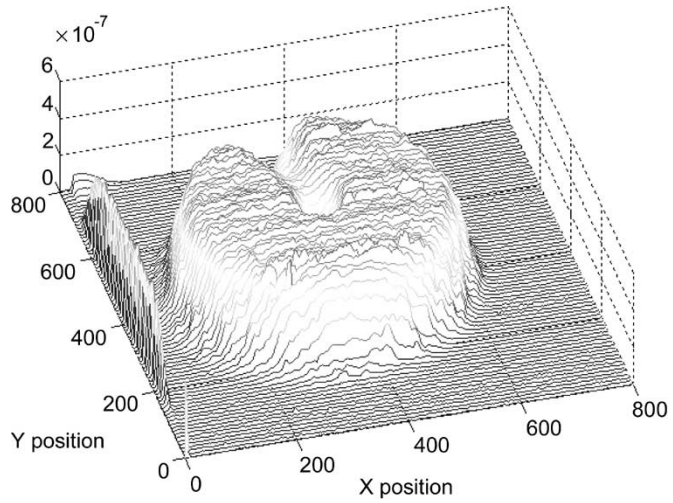

Fig. 6. Spatial photo-response of a 500-μm APD at bias voltage of 38.6 V ($M \geq 20$).

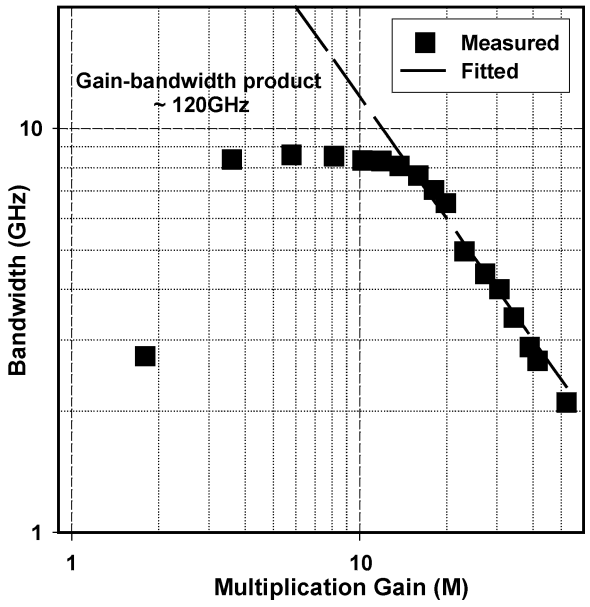

Fig. 7. C–V characteristics of a 50-μm APD array device and a 500-μm large-area APD (shown in the inset).

the array. As described above, the gain was calculated using (1). The mean value of gain was 10.9, 16.1, 22.1, and 43.4 at reverse bias voltages of 35.0, 36.4, 37.2, and 38.2 V, respectively. The standard deviations of the gain distribution at each of the above reverse bias conditions were 0.9, 1.4, 2.1, and 5.6, respectively. These results agree very well with previous 12 × 12 APD array results [11], especially for the high-gain regime.

The bandwidth of the array devices was measured with a HP8703A lightwave component analyzer at the wavelength of 1.3 μm. The bandwidth versus gain is plotted in Fig. 7. The low-gain bandwidth of a typical 50-μm-diameter APD device was ~8 GHz. The bandwidth at low gain was limited by the transit time through the long carrier transport path (~ 3.9 μm) associated with the depleted absorption, charge, and multiplication regions. To verify this, the capacitance of an APD array device was measured versus voltage. For a 50-μm-diameter APD, the measured capacitance was ~125

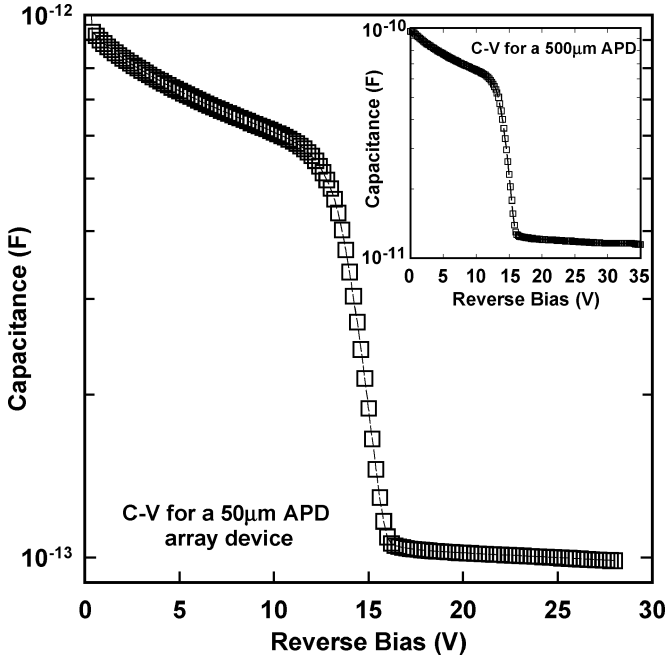

Fig. 8. Bandwidth versus gain for a 50-μm APD array device.

fF ($\sim 6.4 \times 10^{-2}$ fF/μm^2) at low frequency (1 MHz) and at bias voltage of 16.0 V, as plotted in Fig. 8. A capacitance of ~13 pF ($\sim 6.6 \times 10^{-2}$ fF/μm^2) at bias voltage of 16.0 V was also obtained for a 500-μm-diameter device, as shown in the inset of Fig. 8. These measured results are consistent with the calculated capacitance value (6.3×10^{-2} fF/μm^2), and the capacitance was found to be scalable to the mesa area for large-area APDs. The capacitance curve exhibited a sharp decrease before punch-through, but only a slight change was observed after punch-through owing to total depletion of the absorption, charge, and multiplication regions. The capacitance and resistance were also measured with a HP8703A network analyzer with RF calibration frequency up to 10 GHz. The measured capacitance was ~100 fF and total load resistance was $\sim 60\,\Omega$ ($\sim 10\,\Omega$ contact resistance + $50\,\Omega$ terminal resistance). The 3-dB RC-bandwidth was estimated to be >20 GHz using these measured values. The slight discrepancy between the high frequency RF measurement and the low frequency C–V measurement can, at least in part, be attributed to the frequency dependence of the dielectric constant. At higher gains a gain-bandwidth product of 120 GHz was observed. In comparison with previous results [11], the gain-band-width increased ≥5 times due to an improved electric field profile, which reduced the field intensity in the 1500 nm-thick $In_{0.53}Ga_{0.47}As$ absorption region. By increasing the charge layer doping, the electric field strength in the $In_{0.53}Ga_{0.47}As$ absorber decreased from >250 kV/cm to <150 kV/cm at bias voltages close to breakdown.

IV. Conclusion

Large-area mesa $In_{0.53}Ga_{0.47}As$–$In_{0.52}Al_{0.48}As$ APDs have been demonstrated. APDs with mesa diameter of 500 μm exhibited low dark current density of $\sim 2.5 \times 10^{-2}$ nA/μm^2 at 90% of the breakdown. Low surface leakage current density

($\sim$ 4.2 pA/μm) was achieved with wet chemical etching and SiO_2 passivation. An 18 $\times$ 18 APD array has also been demonstrated based on the same material and device structure. This APD array exhibited uniform distributions of breakdown voltage, dark current, and multiplication gain. A bandwidth of $\sim$8 GHz at low gains and a gain-bandwidth product of $\sim$120 GHz were achieved.

REFERENCES

[1] R. S. Balcerak, "Unattended imaging sensors," in *Proc. 3-D Imaging Receivers SPIE Conf.*, Apr. 2000, pp. 11–14.

[2] G. S. Kinsey, J. C. Campbell, and A. G. Dentai, "Waveguide avalanche photodiode with a gain-bandwidth product of 320 GHz," *IEEE Photon. Technol. Lett.*, vol. 13, pp. 842–844, Aug. 2001.

[3] H. S. Kim, J. H. Choi, H. M. Bang, Y. Jee, S. W. Yun, J. Burm, M. D. Kim, and A. G. Choo, "Dark current reduction in APD with BCB passivation," *Electron. Lett.*, vol. 37, no. 7, pp. 455–457, Mar. 2001.

[4] D. Schmidt and D. Trommer, "Conservation of low dark current of InGaAs photodiodes after NH_3F/HF etch a BCB passivation layer," in *Proc. Indium Phosphide and Related Materials Conf.*, pp. 302–305.

[5] M. Hayashi, I. Wantababe, T. Nakata, M. Tsuji, K. Makita, S. Yamakata, and K. Taguchi, "Microlens-integrated large-area InAlGaAs-InAlAs superlattice APDs for eye-safety 1.5-μm wavelength optical measurement use," *IEEE Photon. Technol. Lett.*, vol. 10, pp. 576–578, Apr. 1998.

[6] I. Watanabe, M. Tsuji, M. Hayashi, K. Makita, and K. Taguchi, "Design and performance of InAlGaAs–InAlAs superlattice avalanche photodiodes," *J. Lightwave Technol.*, vol. 15, pp. 1012–1019, June 1997.

[7] C. Cohen-Jonathan, L. Giraudet, A. Bonzo, and J. P. Praseuth, "Waveguide AlInAs/GaAlInAs avalanche photodiode with a gain-bandwidth product over 160 GHz," *Electron. Lett.*, vol. 33, no. 17, pp. 1492–1493, 1997.

[8] H. Nie, K. A. Anselm, C. Lenox, P. Yuan, C. Hu, G. Kinsey, B. G. Streetman, and J. C. Campbell, "Resonant-cavity separate absorption, charge, and multiplication avalanche photodiodes with high speed and high gain-bandwidth product," *IEEE Photon. Technol. Lett.*, vol. 10, pp. 409–411, Mar. 1998.

[9] C. Lenox, H. Nie, P. Yuan, G. Kinsey, A. L. Holmes Jr., B. G. Streetman, and J. C. Campbell, "Resonant-cavity InGaAs-InAlAs avalanche photodiodes with gain-bandwidth product of 290 GHz," *IEEE Photon. Technol. Lett.*, vol. 11, pp. 1162–1164, Sept. 1999.

[10] K. Kato, "Ultrawide-band/high-frequency photodetectors," *IEEE Trans. Microwave Theory Tech.*, vol. 47, pp. 1265–1281, July 1999.

[11] X. G. Zheng, J. Hsu, X. Sun, J. B. Hurst, X. Li, S. Wang, A. L. Holmes Jr., J. C. Campbell, A. S. Huntington, and L. A. Coldren, "A 12 $\times$ 12 $In_{0.53}Ga_{0.47}As$–$In_{0.52}Al_{0.48}As$ avalanche photodiode array," *IEEE J. Quantum Electron.*, vol. 38, pp. 1536–1540, Nov. 2002.

[12] C. Lenox, P. Yuan, H. Nie, O. Baklenov, C. Hansing, J. C. Campbell, A. L. Holmes Jr., and B. G. Streetman, "Thin multiplication region InAlAs homojunction avalanche photodiodes," *Appl. Phys. Lett.*, vol. 73, no. 6, pp. 783–784, 1998.

[13] T. Kagawa, Y. Kawamura, and H. Iwamura, "A wide-bandwidth low-noise InGaAsP-InAlAs superlattice avalanche photodiode with a flip-chip structure for wavelength of 1.3 μm and 1.55 μm," *IEEE J. Quantum Electron.*, vol. 29, pp. 1387–1392, May 1993.

[14] K. Makita, I. Watanabe, M. Tsuji, and K. Taguchi, "Dark current and breakdown analysis in In(Al)GaAs/InAlAs superlattice avalanche photodiodes," *Jpn. J. Appl. Phys.*, vol. 35, pp. 3440–3444, 1996.

X. G. Zheng received the B.S.E.E. degree from the Beijing Institute of Technology, Beijing, China, in 1985, and the M.S. degree in electrical engineering from the Hebei Semiconductor Research Institute in 1991. He is currently pursuing the Ph.D. degree in electrical engineering at the University of Texas at Austin.

His major research areas are in optoelectronic devices, such as impact ionization properties of III-V compound materials, high-speed long-wavelength avalanche photodiodes and arrays, and heterogeneous material integration via direct wafer bonding.

J. S. Hsu received the B.S.E.E. degree from the Pennsylvania State University, University Park, in 1996, and the M.S. Degree in electrical engineering from the University of Texas at Austin in 2002.

Her research includes compound semiconductor avalanche photodetectors operating in the near-infrared long-wavelength regime as well as characterization of avalanche photodetector arrays and large-area avalanche photodetectors.

J. B. Hurst received the B.S. degree in electrical engineering from the University of Oklahoma, Norman, in 1999, and the M.S. degree in electrical engineering from the University of Texas at Austin in 2001. He is currently pursuing the Ph.D. degree at the University of Texas.

His current research interests include molecular beam epitaxy growth of III-V semiconductors, direct wafer bonding, and long-wavelength avalanche photodectectors.

X. Li was born in Beijing, China, in 1970. He received the B.S. and M.S. degrees from the Physics Department, Peking University, Beijing, China, in 1994 and 1997, respectively. He is currently pursuing the Ph.D. degree in electrical engineering at the Microelectronic Research Center, University of Texas at Austin.

His research interests are avalanche process simulations and high-saturation power photodetectors for 1.55–μm applications.

S. Wang received the B.S. degree in microelectronics from Beijing University, Beijing, China, in 1995, and the M.S.E.E. degree from the University of Notre Dame, South Bend, IN, 1999. She is currently pursing the Ph.D. degree at the Microelectronics Research Center, University of Texas at Austin, working on high-speed, low-noise avalanche photodiodes.

Ms. Wang is a student member of the IEEE Lasers and Electro-Optics Society (LEOS).

X. Sun received the B.S. and M.S. degrees in materials science and engineering from Tsinghua University, Beijing, China, in 1995 and 1997, respectively, and the M.S.E.E. degree from the University of Texas at Austin in 2000. He is currently pursing the Ph.D. degree at the Microelectronics Research Center, University of Texas.

His research interests include molecular beam epitaxy growth of III-V compound semiconductors and characterization, and design and fabrication of high-speed near-infrared photodetectors.

Archie L. Holmes, Jr. (M'92) received the B.S.E.E. degree from the University of Texas at Austin in 1991, and the M.S. and Ph.D. degrees in electrical engineering from the University of California, Santa Barbara, in 1992 and 1997, respectively.

He joined the Department of Electrical and Computer Engineering, University of Texas as an Assistant Professor in 1997. His major research areas are in electronic materials and devices, growth of novel semiconductor alloys by molecular beam epitaxy, high-speed photodetectors, and heterogeneous materials integration via direct wafer bonding. He has published more than 80 journal and conference papers.

Dr. Holmes is a member of IEEE Lasers and Electro-Optics Society (LEOS) and the American Society for Engineering Education.

Joe C. Campbell (S'73–M'74–SM'88–F'90) received the B.S. degree in physics from the University of Texas at Austin in 1969, and the M.S. and Ph.D. degrees in physics from the University of Illinois at Urbana-Champaign, in 1971 and 1973, respectively.

From 1974 to 1976, he was employed by Texas Instruments Inc. where he worked on integrated optics. In 1976, he joined the staff of AT&T Bell Laboratories, Holmdel, NJ. In the Crawford Hill Laboratory, he worked on a variety of optoelectronic devices including semiconductor lasers, optical modulators, waveguide switches, photonic integrated circuits, and photodetectors with emphasis on high-speed avalanche photodiodes for high-bit-rate lightwave systems. In January 1989, he joined the faculty of the University of Texas as Professor of electrical and computer engineering and Cockrell Family Regents Chair in Engineering. At present, he is actively involved in Si-based optoelectronics, high-speed, low-noise avalanche photodiodes, high-power photodiodes, ultraviolet photodetectors, and quantum-dot IR imaging. He has coauthored six book chapters, more than 300 journal publications, and 200 conference presentations.

Dr. Campbell is a member of the National Academy of Engineering, a Fellow of the Optical Society of America, and a Fellow of the American Physical Society.

Andrew S. Huntington received the B.S. degree in chemistry from the California Institute of Technology, Pasadena, in 1997. He is currently a graduate student at the Materials Department, University of California at Santa Barbara.

His current research interests are the growth of arsenide compounds lattice-matched to InP for optoelectronic applications, including long-wavelength multiple-active region vertical-cavity lasers and avalanche photodiodes.

Larry A. Coldren (M'72–SM'77–F'82) received the Ph.D. degree in electrical engineering from Stanford University, Palo Alto, CA, in 1972.

After 13 years in the research area at Bell Laboratories, he was appointed Professor of electrical and computer engineering at the University of California at Santa Barbara (UCSB) in 1984. In 1986, he assumed a joint appointment with Materials and Electrical and Computer Engineering, and the Fred Kavli Chair in Optoelectronics and Sensors in 2000. He is also Chairman and Chief Technology Officer of Agility Communications, Inc., Santa Barbara. At UCSB his research efforts have included work on novel guided-wave and vertical-cavity modulators and lasers as well as the underlying materials growth and fabrication technology. He is now investigating the integration of various optoelectronic devices, including optical amplifiers and modulators, tunable lasers, wavelength-converters, and surface-emitting lasers. He has authored or coauthored over 500 papers, five book chapters, and one textbook, and has been issued 32 patents.

Prof. Coldren is a Fellow of the Optical Society of America, a former Vice-President of IEEE Lasers and Electro-Optics Society, and has been active in technical meetings.